The Astrophysical Journal, 805:184 (8pp), 2015 June 1 doi:10.1088/0004-637X/805/2/184

LENS STATISTICS WITH GRAVITATIONALLY LENSED YET MORPHOLOGICALLY REGULAR IMAGES

Masayo Morioka and Toshifumi Futamase
Astronomical Institute, Tohoku University, Aramaki, Aoba, Sendai 980-8578, Japan; mmori@astro.tohoku.ac.jp, tof@astr.tohoku.ac.jp
Received 2014 August 18; accepted 2015 April 9; published 2015 June 2

ABSTRACT

GRAMORs are GRAvitationally highly magnified yet MORphologically regular images. An example of this phenomenon was discovered in the cluster MACS J1149.5+2223 in 2009. We investigate the lens statistics of GRAMORs in detail. Assuming a NFW profile for a sample of clusters, we calculate the expected number and redshift distribution of GRAMORs using parameters from COSMOS data for the number density of the background galaxy. A model with a cluster placed at $z = 0.544$ based on *WMAP5* cosmology predicts the redshift of a GRAMOR at $z \simeq 1.49$ which is close to the observed $z = 1.4906$. These results show that the expected number of GRAMORs is about two per cluster in the most likely case, and thus a large number of GRAMORs would be observed in a systematic survey. The probability distribution function of source redshift for GRAMORs depends strongly on dark energy and may be useful for constraining the nature of dark energy.

Key words: cosmological parameters – galaxies: clusters: general – galaxies: clusters: individual (MACSJ1149.5 +2223) – gravitational lensing: strong

1. INTRODUCTION

Since first being observed (Walsh et al. 1979), strong gravitational lensing has become an important tool for studying various aspects of cosmology (e.g., Gavazzi et al. 2007; Coles 2008; Barnabè et al. 2009). For example, the statistics of strong lensing events are known to have useful information about the evolution of the number density of lensing objects (Mao 1991; Mao & Kochanek 1994; Capelo & Natarajan 2007; Matsumoto & Futamase 2008) as well as cosmological parameters (Turner et al. 1984; Fukugita et al. 1992). In the past, poor and inhomogeneous sampling of images and uncertainty regarding the distribution of the background galaxies prevented the useful application of lens statistics to cosmology. However, recent developments in observational astronomy such as the SDSS (York et al. 2000) and COSMOS projects (Scoville et al. 2007) make the accurate prediction of lens statistics and a detailed comparison with observational data possible (Mitchell et al. 2005; Faure et al. 2008; Oguri et al. 2008) and is expected to continue in the future.

Given this situation, it is worthwhile to study lens statistics from a new point of view. Lens statistics have been studied for quasars (Lopes & Miller 2004; Mitchell et al. 2005; Allen et al. 2008; Oguri et al. 2008) and giant luminous arcs (Turner et al. 1984; Bartelmann 1996; Bartelmann et al. 1998; Oguri et al. 2001; Meneghetti et al. 2013). Here we consider the statistics for GRavitationally highly magnified yet MORphologically regular images (GRAMORs) as predicted by Williams & Lewis (Williams & Lewis 1998) and Futamase, Hattori & Hamana (Futamase et al. 1998). One of the reasons we study GRAMORs is their discovery in the cluster MACS J1149.5+2223 at redshift 0.544 (Zitrin & Broadhurst 2009). The image is a spiral galaxy at redshift 1.4906 with area 55□″ and is observed near the center of the cluster as one of multiple images. The area of all lensed images covers 150□″ with a magnification estimated to be ∼200 in total. Mass reconstruction using multiple images showed a very flat mass profile (Smith et al. 2009; Zitrin & Broadhurst 2009). This fact is consistent with the theoretical prediction that a mass distribution with a flat central core can easily produce undistorted images (Futamase et al. 1998; Williams & Lewis 1998). The other reason is the expectation that the statistics of GRAMORs will depend strongly on cosmological parameters. Lens statistics depends in general on the cosmological parameters, in particular the existence of dark energy (Fukugita et al. 1990; Hamana et al. 1997; Futamase et al. 1998). In the case of GRAMORs, the conditions needed for their formation is more strict compared with giant luminous arcs, and thus the appropriate combination of cosmological parameters will be more restricted. Since the statistics depend not only on the cosmological parameters but also on the lensing object and background source, it is crucial to use realistic models for the lensing object and sources to make a realistic prediction. We shall make use of the observed sample of clusters (LoCuSS sample) as our model of lensing clusters (Okabe et al. 2010) and COSMOS data for the number density of the background galaxies (Fu et al. 2008; Ilbert et al. 2009). We find that this expectation is, in fact, the case.

This paper is organized as follows. In Section 2, we describe the basic properties of the NFW lens model and give the definition of GRAMORs. In Section 3 we summarize the observed GRAMOR based on previous work. In Section 4 we describe our calculation of the lens statistics and the assumptions in detail. The results of the calculation are given in Section 5 where we will show the dependence of the results on the lens model and redshift. In particular we will find a strong dependence on dark energy. Finally, the conclusions and discussion are presented in Section 6.

Throughout this paper we use the cosmological parameters taken from *WMAP5* data, $(\Omega_m,\Omega_\Lambda) = (0.27, 0.73)$, $H_0 = 100\,h^{-1}\,\mathrm{km\,s^{-1}\,Mpc^{-1}}$, and $h = 0.73$ unless otherwise noted.

2. BASIC KNOWLEDGE OF THE GRAVITATIONAL LENSING

2.1. Basic Equations

The basic equation of gravitational lensing is the lensing equation,

$$\boldsymbol{\beta} = \boldsymbol{\theta} - \boldsymbol{\alpha}(\boldsymbol{\theta}), \tag{1}$$

where $\boldsymbol{\beta}$ is the 2D angular position vector in the source plane, $\boldsymbol{\theta}$ is the 2D angular position vector in the image plane and $\boldsymbol{\alpha}$ is the deflection angle projected onto the sky. For the spherical lens model, we can write the deflection angle simply using the mass $M(<\theta)$ enclosed within the radius θ as follows.

$$\boldsymbol{\alpha} = \frac{4G}{c^2}\frac{D_d D_{ds}}{D_s} M(<\theta)\frac{\boldsymbol{\theta}}{\theta^2} \tag{2}$$

where $M(<\theta)$ is the integrated surface mass density $\Sigma(\theta)$,

$$M(<\theta) = \int_0^\theta 2\pi\theta'\Sigma\left(\theta'\right)d\theta'. \tag{3}$$

Here, we introduce the convergence κ, the dimensionless surface mass density,

$$\kappa(\theta) = \frac{\Sigma(\theta)}{\Sigma_{\rm cr}}, \tag{4}$$

with $\Sigma_{\rm cr}$ the critical surface mass density defined by

$$\Sigma_{\rm cr} = \frac{c^2}{4\pi G}\frac{D_s}{D_d D_{ds}}, \tag{5}$$

where D_d, D_s and D_{ds} are the angular diameter distances from the observer to the lens, from the observer to the source and from the lens to the source, respectively.

Using these parameters, we can write the enclosed mass and the lens equation for a spherical lens model with κ. Next, we consider the eigenvalues of the Jacobian matrix A. For the circular lens model, the eigenvalues are expressed

$$\lambda_- = 1 - \kappa - \gamma \tag{6}$$

$$= 1 + \frac{1}{\pi\Sigma_{\rm cr}}\left(\frac{M(<\theta)}{\theta^2} - \frac{1}{\theta}\frac{dM(<\theta)}{d\theta}\right) \tag{7}$$

$$\lambda_+ = 1 - \kappa + \gamma = 1 - \frac{1}{\pi\Sigma_{\rm cr}}\frac{M(<\theta)}{\theta^2}. \tag{8}$$

2.2. NFW Lens Model

We use the NFW profile (Navarro et al. 1997) as the lens model. The density profile is given by the following formula,

$$\rho = \frac{\rho_{\rm crit}\delta_c}{x(1+x)^2}, \tag{9}$$

where $\rho_{\rm crit} = 3H^2/8\pi G$ is the critical density, x is the radius in units of a scale radius r_s, $x \equiv r/r_s$, and δ_c is a characteristic overdensity and defined as

$$\delta_c = \frac{200}{3}\frac{c^3}{\ln(1+c) - c/(1+c)}, \tag{10}$$

$c = r_{200}/r_s$ is called the concentration parameter and r_{200} is the radius within which the density is higher than 200 times the averaged density. The lens equation of the NFW profile becomes

$$y = x - \frac{m(x)}{x}, \tag{11}$$

where $y = (\eta/r_s)(D_d/D_s)$, η is the position vector in the source plane, and $m(x)$ is the projected dimensionless mass profile

$$m(x) \equiv 2\int_0^x y\kappa(y)dy. \tag{12}$$

From Equation (9), the surface mass density is expressed

$$\Sigma(x) = \frac{2\rho_s r_s}{x^2-1}f(x), \tag{13}$$

with

$$f(x) = \begin{cases} 1 - \dfrac{2}{\sqrt{x^2-1}}\arctan\sqrt{\dfrac{x-1}{x+1}} & (x>1) \\ 0 & (x=1) \\ 1 - \dfrac{2}{\sqrt{1-x^2}}\mathrm{arctanh}\sqrt{\dfrac{1-x}{1+x}} & (x<1). \end{cases} \tag{14}$$

Therefore, the convergence can be written

$$\kappa(x) = 2\kappa_s\frac{f(x)}{x^2-1} \tag{15}$$

where $\kappa_s \equiv \rho_s r_s/\Sigma_{\rm crit}$. Inserting Equation (20) into (12), the dimensionless mass $m(x)$ becomes

$$m(x) = 4\kappa_s g(x), \tag{16}$$

where

$$g(x) = \ln\frac{x}{2} + \begin{cases} \dfrac{2}{\sqrt{x^2-1}}\arctan\sqrt{\dfrac{x-1}{x+1}} & (x>1) \\ 1 & (x=1) \\ \dfrac{2}{\sqrt{1-x^2}}\mathrm{arctanh}\sqrt{\dfrac{1-x}{1+x}} & (x<1). \end{cases} \tag{17}$$

3. GRAMORS

3.1. The Definition of GRAMORs

GRAMORs means GRAvitationally highly magnified yet MORphologically regular images. We define a GRAMOR using the distortion parameter R and the magnification parameter A. These are defined by the eigenvalues of the Jacobian, λ_- and λ_+ as follows.

$$R = \frac{\lambda_-}{\lambda_+} \tag{18}$$

and

$$A = \frac{1}{\lambda_-\lambda_+}. \tag{19}$$

A GRAMOR is then defined as images which satisfy the condition $1/3 \leqslant R \leqslant 3$ and $10 \leqslant A$. We adopt the above definition based on previous reports (Futamase et al. 1998; Williams & Lewis 1998).

3.2. The Observed GRAMOR

The first GRAMOR was discovered by Zitrin and Broadhurst in 2009 in the center of MACS J1149.5+2223. Here we summarize the properties of the observed GRAMOR. It is

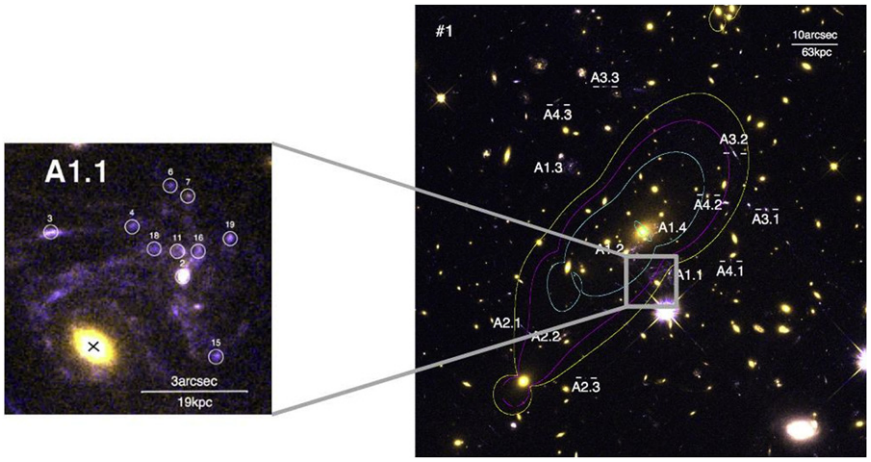

Figure 1. Image of the observed GRAMOR. This figure is excerpted from Smith et al. (2009).

observed in the center of MACS J1149.5+2223, an X-ray luminous cluster at $z = 0.544$. The image is one of multiple images of a blue spiral galaxy at $z = 1.4906$. It covers an area of $\simeq 55\square''$ and magnification is estimated to be $\mu = 23$. An image of the observed GRAMOR is shown in Figure 1, cited from Smith et al. (2009).

According to the lens model of Zitrin and Broadhurst, the diameter of the source for the GRAMOR is about 0.″5. However, the size of the massive galaxies at $z \sim 1.5$ is about $1''$ (Trujillo et al. 2007). Thus the source of the observed GRAMOR is not a special galaxy. The reconstructed mass distribution by Smith et al, MACS J1149.5+2223, shows a very flat core with a profile expressed by $\kappa \sim \theta^{\gamma}$, where θ is the position angle in the lens plane and $\gamma \sim -0.3 \pm 0.05$ in the range $3'' \leqslant \theta \leqslant 30''$. This range corresponds to $19\,\mathrm{kpc} \leqslant r \leqslant 190\,\mathrm{kpc}$, where r is the distance from the cluster center in the lens plane.

In order to use this profile as a lens model in later calculations, we determine the proportional coefficient of the power law θ^{γ}.

$$\kappa = K(z_s)\theta^{-0.3} \tag{20}$$

where the proportional constant K has a source redshift dependence. By comparing Equation (20) with Figure 4 in Smith et al. (2009), we obtain $K_{1.5} \equiv K(z_s = 1.5) = 1.905$. Since the convergence has a redshift dependence D_{ds}/D_s, we have

$$K(z) = K_{1.5}\frac{D_{ds}(z)/D_s(z)}{D_{ds}(z_s = 1.5)/D_s(z_s = 1.5)} = 3.5\frac{D_{ds}}{D_s}. \tag{21}$$

This is expressed in arcseconds. By transforming into radians, we use the following form for the lens profile of MACSJ1149.5 +2223 in Section 5.

$$\kappa = 0.089\frac{D_{ds}}{D_s}\theta_{\mathrm{rad}}^{-0.3}. \tag{22}$$

4. ANALYSIS

4.1. Lens Statistics

In order to determine the expected number of GRAMORs, we introduce the cross section σ_s in the source plane in such a way that the source within the cross section makes a GRAMOR. The cross section σ_s depends on the properties of lens and sources. Then the number of GRAMORs produced by the sources between redshift z and $z + dz$ is given by

$$\begin{aligned} dN(z_s) &= n(z_s)\sigma_s\frac{cdt}{dz_s}dz_s \\ &= n(z_s)\sigma_s\frac{c}{H_0}\frac{dz_s}{(1+z_s)\sqrt{\Omega_0(1+z_s)^3 + \Omega_\Lambda}}, \end{aligned} \tag{23}$$

where $n(z_s)$ is the number density of the sources as a function of redshift. Ω_0 and Ω_Λ are the matter density parameter and the dark energy density parameter respectively. The total number of images is obtained by integrating dN from z_s to $z = \infty$.

$$\begin{aligned} N &= \int dN \\ &= \int_{z_l}^{\infty} n(z_s)\sigma_s\frac{c}{H_0}\frac{dz_s}{(1+z_s)\sqrt{\Omega_0(1+z_s)^3 + \Omega_\Lambda}}. \end{aligned} \tag{24}$$

We define the probability distribution function (PDF) $P(z_s)$ of the source redshift as normalized by the total number of the expected number of GRAMORs.

$$P(z_s) = \frac{N(z_s)}{N}. \tag{25}$$

This PDF will be used for comparing the results using various sets of cosmological parameters.

4.2. Sample of Clusters

As our lens model, we choose four cluster models suggested by weak lensing observations of 52 LoCuSS clusters (Okabe et al. 2010) which is a sample of X-ray clusters with redshifts from 0.15 to 0.3. Based on the results of Okabe et al., we selected 48 out of 52 clusters which are well described by an NFW profile, and are then classified into four types, A to D, based on mass as shown in Table 1. In the table, each type of model cluster is obtained by stacking 12 clusters to get the average density profile with the average mass and concentration parameter. Figure 2 shows the density profiles for these four types of clusters. We set the lens redshift $z_l = 0.2$ for all clusters. The smaller the concentration parameter the clusters have, the more flat mass distribution they have, as expected from the definition of the concentration parameter.

Table 1
Parameters of the Four Lens Models Used

Cluster Type	$M_{\rm vir}$ ($10^{14}\,h^{-1}\,M_{\rm Sun}$)	r_s (h^{-1} kpc)	c
A	3.230	217.41	5.762
B	6.011	350.98	4.419
C	7.587	387.06	4.299
D	12.678	537.83	3.663

Note. $M_{\rm vir}$ is the virial mass, r_s is the scale radius and c is the concentration parameter.

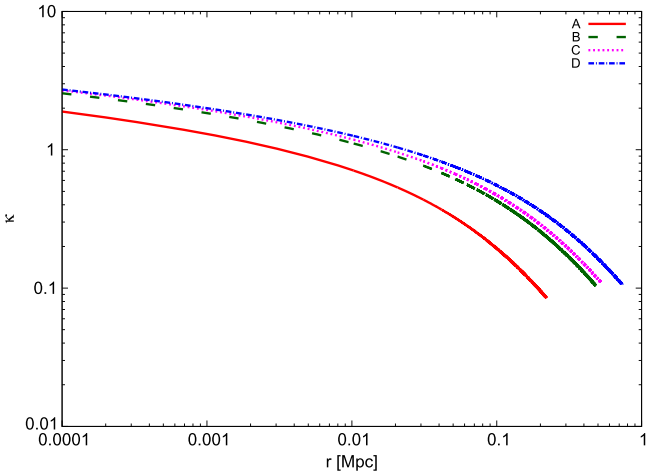

Figure 2. Convergence profiles of the four types of clusters evaluated. The solid, dashed, dotted and dotted–dashed lines show results with lens models A, B, C and D, respectively. Lens models with smaller concentration parameters have flatter profiles.

4.3. The Source Distribution

The source redshift distribution is needed for calculation of the expected number of images. We use the best-fit function from the COSMOS survey proposed by Ilbert et al. (2009).

$$n(z) = A\frac{z^a + z^{ab}}{z^b + c} \tag{26}$$

with

$$A = \left(\int_0^\infty \frac{z^a + z^{ab}}{z^b + c} dz \right)^{-1}. \tag{27}$$

A is the normalization factor and a, b, c are free parameters. The best-fit parameters are obtained for each bin from $22 < i^+ < 22.5$ to $24.5 < i^+ < 25$ and these parameters are shown in Table 2 of Ilbert et al. (2009). By adding all distributions, we get the galaxy redshift distribution for $22 < i^+ < 25$. This is shown in Figure 3. We use this distribution as the number density of the source, $n(z_s)$, when we calculate the expected number of GRAMORs.

5. RESULTS

In this section we present the results of the calculations. The results depend on the lens model used, the definition of GRAMORs, the lens redshift and the cosmological parameters. We will explain each of these dependencies.

Here, we consider the detectability in terms of the source size. As mentioned in Section 2, the source size of the observed

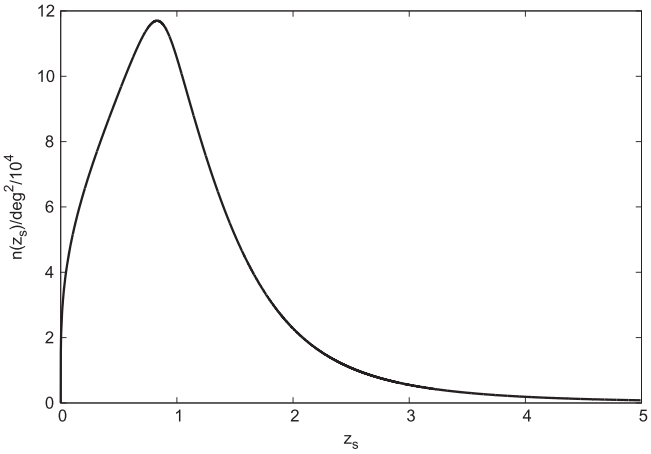

Figure 3. Distribution of the background galaxies derived from COSMOS data.

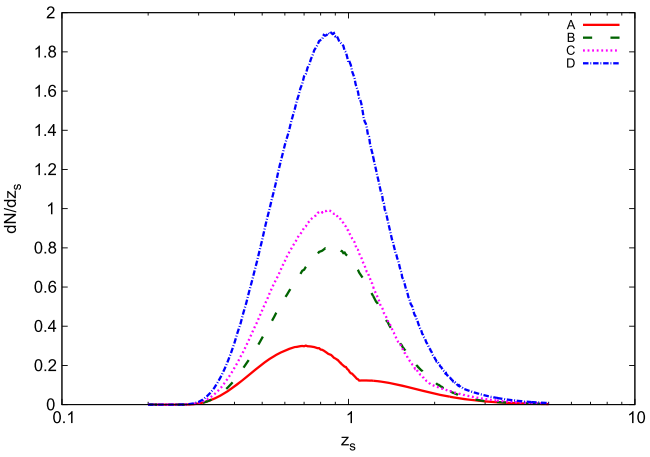

Figure 4. Expected distributions for the four types of clusters evaluated, including Types A, B, C and D. The type and color of the lines follow the same description as in Figure 2.

GRAMOR is about 0.″5. However, the size of the massive galaxies at $z \sim 1.5$ is about 1″ (Trujillo et al. 2007). This means that the source of the observed GRAMOR is not special compared with that of other galaxies at $z \sim 1.5$. In summary, the size of the GRAMOR's source does not lead to a problem regarding detectability.

5.1. Dependence on Lens Model Parameters

We first calculate the expected number distributions of GRAMORs for four types of clusters at $z = 0.2$ by fixing the other parameters. The result is shown in Figure 4. From this figure, we find that a cluster with a smaller concentration parameter tends to produce more GRAMORs than one with a higher concentration parameter. This means that it is easier to observe GRAMORs in clusters with a mass distribution that is flat near the center. This is consistent with the fact that a cluster mass profile with a flat central core can easily give rise to an undistorted images as pointed out in earlier studies (Futamase et al. 1998; Williams & Lewis 1998).

5.2. Dependence on Lens Redshift

We shall now consider the dependence of the expected number of GRAMORs on lens redshift. We choose $z_l = 0.2$,

Table 2
The Expected Number of GRAMORs for Each Model

z_l	0.2	0.3	0.544	0.7
A	0.295387	0.601859	0.323144	0.161944
B	0.800333	0.798691	0.927403	0.479386
C	0.931151	1.174562	1.111886	0.564208
D	1.851518	1.998245	2.170035	1.114325

0.3, 0.544, and 0.7. $z_l = 0.544$ is the redshift of MACS J1149.5 +2223 in which a GRAMOR has been observed. Table 2 shows the expected number for each lens model and each lens redshift. From this table, we find a strong dependence on the lens redshift for any lens model. In particular, GRAMORs are likely to be observed for the lens models B and D at $z_l = 0.544$ and rarely observed for lens model A at any redshift. Thus, we further consider lens models B and D to investigate other dependencies of the expected number. We show the lens redshift dependence in Figure 5. which clearly shows a strong dependence on source redshift. In particular, the distribution in the case of $z_l = 0.544$ has a sharp peak at $z_s \sim 1.49$ for lens model D which is close to the observed redshift $z = 1.4907$.

Some of the distributions have two peaks which comes from the fact that there are two conditions that result in a GRAMOR. This result also shows that we can observe a sufficient number of GRAMORs to be used for lens statistics if a systematic survey for clusters with a relatively low concentration parameter is performed. The observational strategy will be mentioned later.

5.3. Dependence on the Definition of GRAMORs

Next we consider how the definition of GRAMORs changes the results. So far, GRAMORs are defined as an image that has $1/3 \leqslant R \leqslant 3$ and $10 \leqslant A$ as stated above. In this section, we compare the expected number distribution for images that have different conditions for magnification, $10 \leqslant A$, $20 \leqslant A$ and $30 \leqslant A$. The result is shown in Figure 6. Distributions with a larger magnification have peaks at a lower redshift. This comes from the fact that images at the higher redshift are too strongly distorted, so they do not satisfy the condition for distortion. The total numbers of observable GRAMORs are $N_{A\geqslant 10} = 2.170335$, $N_{A\geqslant 20} = 0.099358$, $N_{A\geqslant 30} = 0.012873$, respectively. Thus, highly magnified GRAMORs are very rare. However, if they are observed, they will constrain cosmological parameters much more severely as suggested by the argument below.

5.4. Dependence on the Cosmological Constant

As expected from the quasar statistics, GRAMOR statistics may have a strong dependence on the cosmological parameters. Here we concentrate on the dependence of lens statistics specifically on the cosmological constant. We also assume a totally flat geometry.

We calculate the PDF with three cosmological parameter sets, an Einstein–de Sitter (EdS) universe, $(\Omega_m, \Omega_\Lambda, h) = (1, 0, 0.73)$ the universe based on *WMAP*5 data, $(\Omega_m, \Omega_\Lambda, h) = (0.24, 0.73, 0.73)$ and the universe based on Planck13 data, (Planck Collaboration et al. 2014), $(\Omega_m, \Omega_\Lambda, h) = (0.3175, 0.6825, 0.6711)$. The results are shown in Figure 7, where we consider types B and D at $z_l = 0.544$ as typical examples.

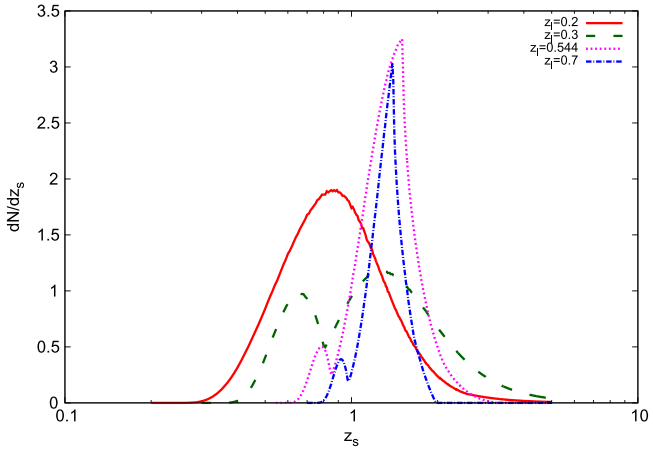

Figure 5. Dependence on the lens redshift shown for the type D lens model. The solid line, dashed line, dotted line and dotted–dashed line show the results with $z_l = 0.2$, $z_l = 0.3$, $z_l = 0.544$ and $z_l = 0.7$, respectively.

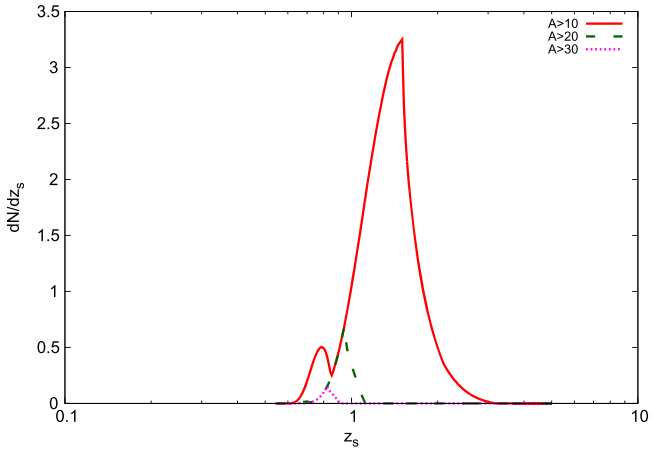

Figure 6. Dependence on the definition of GRAMORs is shown. The expected number is getting smaller with a more strict definition based on the value of the magnification parameter, A. The solid line, dashed line and dotted line represent the conditions of A, $A \leqslant 10$, $A \leqslant 20$ and $A \leqslant 30$, respectively.

From this figure, one can immediately see differences between the three cosmologies. First, the peak shapes are different. For the EdS universe, the peak is higher and narrower than the others. Second, the peak redshifts are different. This figure indicates that if we find a GRAMOR with redshift $z_s \sim 1.5$ in a cluster at $z_l = 0.544$, the EdS universe will be rejected with a high probability. Furthermore, the shapes of the peaks have a non-negligible difference between *WMAP* cosmology and Planck cosmology. Thus if we observe a large number of GRAMORs and their redshift distribution, more stringent constraints for the cosmological constant will be obtained by combining them with other observations such as CMB, and BAO. We will come back to this point later using a more realistic lens model for the cluster MACS J1149.5+2223 in the next subsection.

This is a unique property of GRAMORs. In fact if we perform the same calculation for an arc with the definition of an arc being $R \geqslant 10$, then the result is as shown in Figure 8. The conditions of the calculation are same as that for GRAMORs, but there are no big differences in the peak positions between the two types of cosmological models for the arc. The reason for this difference may be found in the dependence of the distortion parameter R and the magnification parameter A on

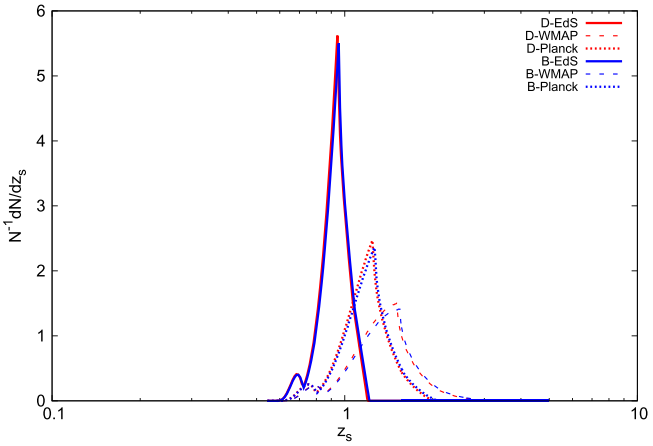

Figure 7. Dependence on the cosmological parameter for GRAMORs is shown. We employ three sets of cosmological parameters, based on the Einstein–de Sitter universe, *WMAP* data and Planck data for lens types D and B. The plots show the normalized expected number distributions plotted against the total number, resulting in a probability distribution function (PDF) of source redshift for GRAMORs. The solid lines, dashed lines and dotted lines represent the EdS, *WMAP*5 and Planck data respectively. The red lines represent lens model D and the blue lines represent lens model B. The behaviors of the PDFs are similar regardless the lens type.

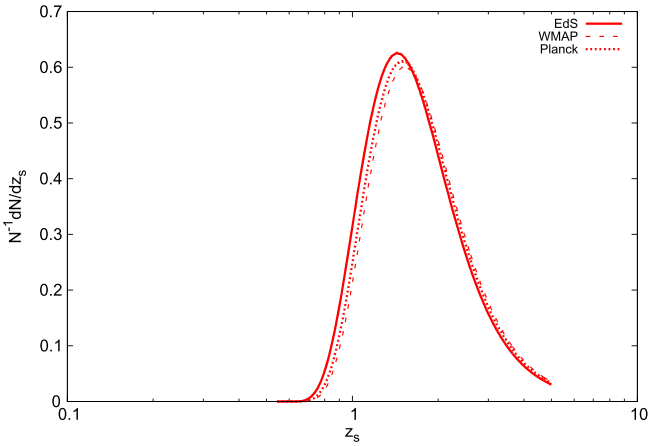

Figure 8. Dependence on the cosmological parameter for arcs for lens model D is shown. The color and type of the line and the cosmological parameters used are the same—bf with those used in Figure 7.

the cosmological parameters. The parameter used for defining the arc is only R and the behavior of R in the EdS and ΛCDM universes is shown in Figures 9 and 10 respectively. The color of the line corresponds to the redshift of the source. In both cases, the area where images are distorted becomes larger and moves to outside the lens as the source redshift increases. The increasing rate of the area with $10 \leqslant R$ is not so different in the two types of cosmology. The size of the area is different but it does not have a big effect because the final result is normalized. Likewise, the dependence of the expected number of arcs on cosmological parameters is not so strong.

However, the behavior of A with EdS cosmological parameters changes rapidly. Figures 11 and 12 illustrate this property. Even if the source redshift is low, the area where the condition $10 \leqslant A$ is satisfied decreases as the source redshift becomes higher. It is easy to understand this by comparing with the graph of $z_s = 1.5$. The range of values that satisfy $10 \leqslant A$ in the EdS universe is about $0.17 \leqslant x \leqslant 0.22$, while that for ΛCDM is about $0.08 \leqslant x \leqslant 0.4$. Thus, the rate of change for A in the EdS universe is greater than that for ΛCDM. This leads to the result that the PDF calculated based on the EdS universe is limited to the low redshift range.

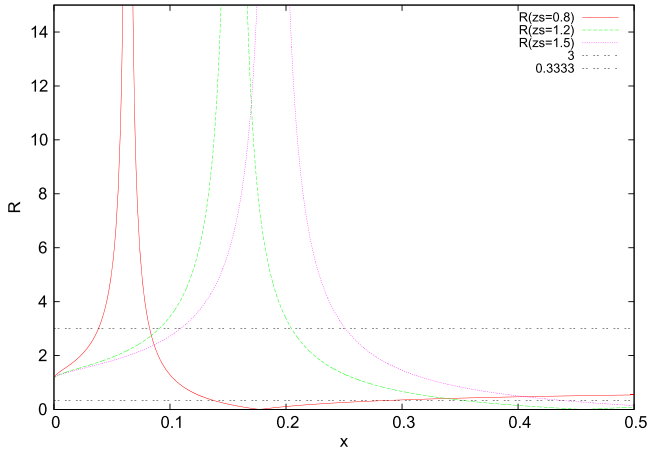

Figure 9. Behavior of R in the Einstein–de Sitter universe with changing source redshifts. The abscissa is the lens radius in units of scale radius, $x \equiv r/r_s$. The solid line, dashed line and dotted line represent $z_s = 0.8$, $z_s = 1.2$ and $z_s = 1.5$, respectively. The horizontal lines show the upper and lower limits of R for the definition of GRAMORs.

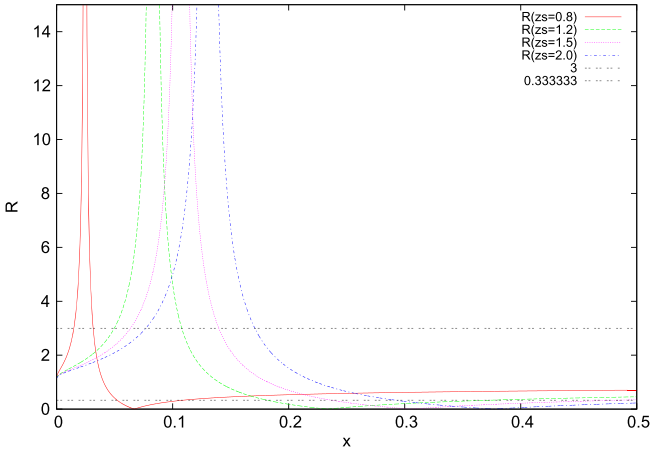

Figure 10. Graph using the same conditions as in Figure 9, but we use the ΛCDM universe and add the results with $z_s = 2.0$.

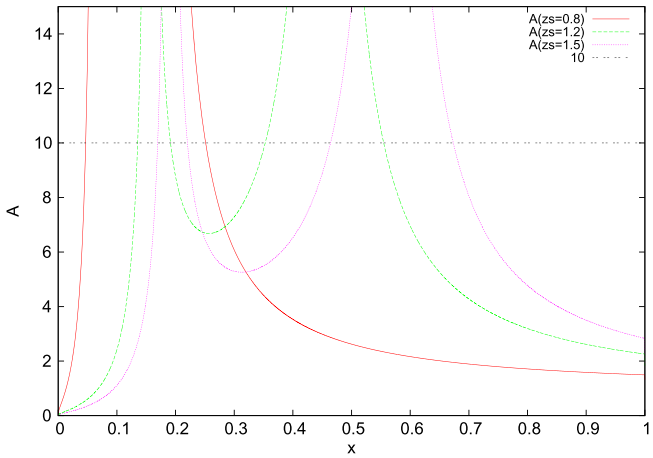

Figure 11. Behavior of A with the Einstein–de Sitter universe model. The lines are the same as in Figure 9. The horizontal line is the lower limit of A for the definition of GRAMORs.

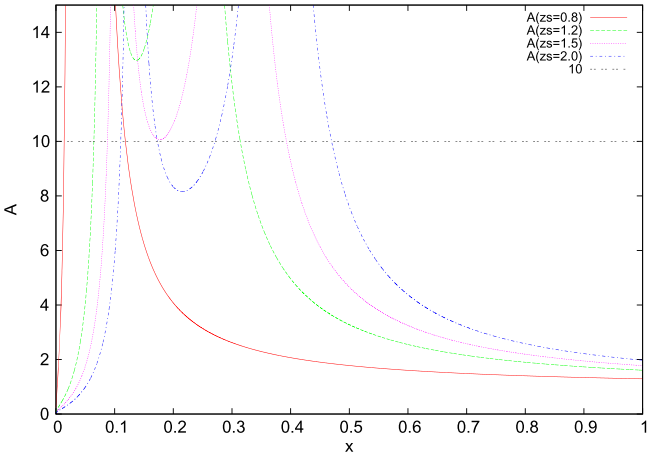

Figure 12. Graph using the same conditions as in Figure 11, but we use the ΛCDM universe and add the results with $z_s = 2.0$.

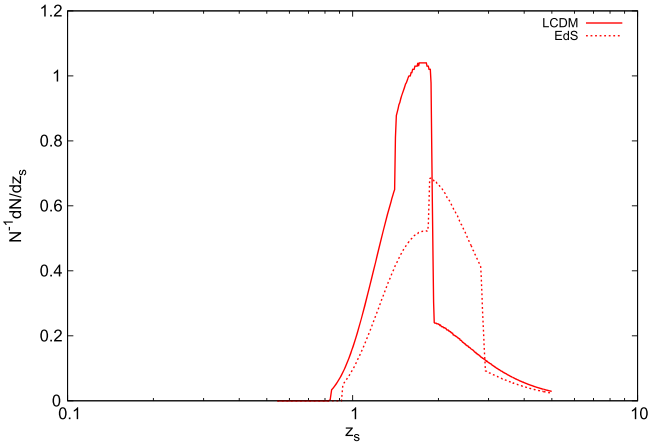

Figure 13. PDFs with the profile of MACSJ1149.5+2223. The solid line and dotted line represent the the ΛCDM and Einstein–de Sitter universes respectively.

In short, the reason why there is a big difference in the dependence on cosmological parameters of the PDFs between arcs and GRAMORs is that a GRAMOR has a dependence on A, but an arc does not.

5.5. MACSJ1149.5+2223

MACSJ1149.5+2223 is currently the only known cluster in which a GRAMOR has been observed. Here, we apply our calculation to this cluster. We use Equation (22) as the profile of MACSJ1149.5+2223 derived in Section 3 and set $z_l = 0.544$ and $22 \leqslant A \leqslant 24$. Regarding the observed GRAMOR, the magnification is estimated to be $A = 23$ although there is no data for R although it looks nearly face-on. We will set only the magnification limit here.

We use the two cosmological models ΛCDM and EdS, as in the case of calculations with the NFW profile. Figure 13 shows the PDFs calculated with each cosmology. As shown in Figure 13, there are large differences between the two cases. We focus on the region around $z_s \sim 1.49$, which is the source redshift of the observed GRAMOR. In this region, the possibility in the case of the ΛCDM universe is about twice as high as that in the case of the EdS universe. The peak position of the PDF is at around $z_s \sim 1.6$ in the ΛCDM case, and about $z_s \sim 2$ in the EdS case. Thus, the ΛCDM universe is more preferable compared to the EdS universe. According to the HFF project, there have been 38 lensed images in 13 families in MACS J1149.5+2223 observed in addition to the GRAMOR by *Hubble Space Telescope* (http://www.stsci.edu/hst/campaigns/frontier-fields/). If we use these images in addition to the observed GRAMOR, we would get more severe constraints, which is the subject of a future study. A more detailed study of this GRAMOR and its dependence on the cosmological parameters using a realistic mass reconstruction for MACS J1149.5+2223 will be presented elsewhere (A. T. Lefor et al. 2015, in preparation)

6. DISCUSSION AND CONCLUSIONS

In this paper, we studied the lens statistics for GRAMORs, which are gravitationally highly magnified yet morphologically regular images. We calculated the expected number distribution of GRAMORs as a function of source redshift changing several conditions.

First, we used four types of lens model with an NFW profile suggested by weak lensing studies of the LoCuSS clusters. The dependence on the mass profile, especially the concentration parameter, becomes clear. The cluster with a flat core produces more GRAMORs which is consistent with previous investigations.

Second, we consider various values of lens redshift and found that the distribution has a sharp peak in most cases. In particular the peak becomes more sharp for clusters with a higher redshift. We also found that the number of GRAMORs is expected to be ∼2.1 per cluster in the most likely case. This means that a sufficient number of GRAMORs can be expected to be observed based on the statistics if we perform a systematic survey.

We then consider GRAMOR statistics for three types of cosmological models, the EdS universe, universes with parameters obtained using *WMAP* data, and those using Planck data. We find that the expected number of GRAMORs and their distribution depends strongly on the cosmological parameters. This suggests a possible method to constrain the value of the cosmological constant. Namely by observing a large number of GRAMORs and their redshift distributions, a stringent constraint for the cosmological constant will be obtained by combining this data with other observations such as CMB and BAO. Although we consider the case of the cosmological constant for simplicity, we expect that this method using GRAMORs may be useful to study the properties of dark energy as well.

We also calculated the PDF in a model of MACSJ1149.5 +2223 with two cosmological models. The result shows a large difference between the two models. The peak position in the PDF is at about $z = 1.6$ for the ΛCDM universe which is close to the observed value of $z_s = 1.4906$, while the PDF has a peak at about $z_s = 2$ in the EdS model. It is rather surprising that only one system MACSJ1149.5+2223 and one image can result in a strong constraint on the existence of the cosmological constant.

Finally we describe an observational strategy to identify GRAMORs. Since GRAMORs are likely to be observed in clusters of galaxies with relatively low concentration and the source redshift dependence is sharply peaked for high-z clusters, we first make a sample of such clusters with $z > 0.5$, for example. Then the peak of the source redshift

distribution is at approximately $z = 1.5$ depending on the cosmology. High-resolution multi-color imaging and/or an infrared narrow band filter should be used to identify GRAMORs. By performing multi-color imaging, we can select the source galaxies which exist around the peak of the source redshift distribution. Planned space satellites such as *James Webb Space Telescope (JWST)*, WFIRST, EUCLID, WISH are most appropriate for such a survey.

We thank K. Umetsu and Y. Okura for many helpful suggestions and useful discussions. We also thank N. Okabe for providing the cluster date and helpful suggestions. Finally we thank Alan Lefor for useful discussions and improving the English usage. This work is supported in part by Grant-in-Aid from Science and Research Council (No. 26400264 for T.F.).

REFERENCES

Allen, S. W., Rapetti, D. A., Schmidt, R. W., et al. 2008, MNRAS, 383, 879
Barnabè, M., Czoske, O., Koopmans, L. V. E., et al. 2009, MNRAS, 399, 21
Bartelmann, M. 1996, A&A, 313, 697
Bartelmann, M., Huss, A., Colberg, J. M., Jenkins, A., & Pearce, F. R. 1998, A&A, 330, 1
Capelo, P. R., & Natarajan, P. 2007, NJPh, 9, 445
Coles, J. 2008, ApJ, 679, 17
Faure, C., Kneib, J.-P., Covone, G., et al. 2008, ApJS, 176, 19
Fu, L., Semboloni, E., Hoekstra, H., et al. 2008, A&A, 479, 9
Fukugita, M., Futamase, T., & Kasai, M. 1990, MNRAS, 246, 24P
Fukugita, M., Futamase, T., Kasai, M., & Turner, E. L. 1992, ApJ, 393, 3
Futamase, T., Hattori, M., & Hamana, T. 1998, ApJL, 508, L47
Gavazzi, R., Treu, T., Rhodes, J. D., et al. 2007, ApJ, 667, 176
Hamana, T., Hattori, M., Ebeling, H., et al. 1997, ApJ, 484, 574
Ilbert, O., Capak, P., Salvato, M., et al. 2009, ApJ, 690, 1236
Lopes, A. M., & Miller, L. 2004, MNRAS, 348, 519
Mao, S. 1991, ApJ, 380, 9
Mao, S. D., & Kochanek, C. S. 1994, MNRAS, 268, 569
Matsumoto, A., & Futamase, T. 2008, MNRAS, 384, 843
Meneghetti, M., Bartelmann, M., Dahle, H., & Limousin, M. 2013, SSRv, 177, 31
Mitchell, J. L., Keeton, C. R., Frieman, J. A., & Sheth, R. K. 2005, ApJ, 622, 81
Navarro, J. F., Frenk, C. S., & White, S. D. M. 1997, ApJ, 490, 493
Oguri, M., Taruya, A., & Suto, Y. 2001, ApJ, 559, 572
Oguri, M., Inada, N., Strauss, M. A., et al. 2008, AJ, 135, 512
Okabe, N., Takada, M., Umetsu, K., Futamase, T., & Smith, G. P. 2010, PASJ, 62, 811
Planck Collaboration, Ade, P. A. R., Aghanim, N., et al. 2014, A&A, 571, AA16
Smith, G. P., Ebeling, H., Limousin, M., et al. 2009, ApJL, 707, L163
Scoville, N., Aussel, H., Brusa, M., et al. 2007, ApJS, 172, 1
Trujillo, I., Conselice, C. J., Bundy, K., et al. 2007, MNRAS, 382, 109
Turner, E. L., Ostriker, J. P., & Gott, J. R., III 1984, ApJ, 284, 1
Walsh, D., Carswell, R. F., & Weymann, R. J. 1979, Natur, 279, 381
Williams, L. L. R., & Lewis, G. F. 1998, MNRAS, 294, 299
York, D. G., Adelman, J., Anderson, J. E., Jr., et al. 2000, AJ, 120, 1579
Zitrin, A., & Broadhurst, T. 2009, ApJL, 703, L132